Numerical comparison between conventional and interdigitated flow fields in Proton Exchange Membrane Fuel Cells (PEMFCs)

Giuseppe Corda[1,*], *Alessandro* d'Adamo[1], and *Matteo* Riccardi[1]

[1] *Department of Engineering "Enzo Ferrari", University of Modena and Reggio Emilia, Via Vivarelli 10, Modena 41125, Italy*

Abstract. The recent trend towards the decarbonization of the energy system has renewed the scientific community's interest in fuel cells. These devices have the potential to eliminate, or greatly reduce, the production of greenhouse gases. Polymeric Electrolyte Membrane Fuel Cells (PEMFC) are among the most promising technologies in this regard, being suited for various applications in stationary power plants, vehicles, and portable power devices. The critical issues in PEMFC are the limitation of oxygen transport through the air cathode and water management at high current density operation, which could be largely limited by modifying the design of the reactant supplier channels. In this paper, a three-dimensional CFD approach is used to compare straight and interdigitated flow fields, focusing on the increased current density and improved water management in the diffusion and catalyst layers for the interdigitated design. The simulation results show that the fluid is forced to flow through the porous layers, promoting a convection-type transport, leading to better water removal from the porous layers as well as to increased transport rates of reactants/products to/from the catalyst layers.
This leads to reduced concentration overpotentials, and it shows the potential of simulation-driven design for high energy density PEMFC systems.

Introduction

Proton-exchange membrane fuel cells (PEMFCs) have recently attracted the attention of the transport sector as a viable alternative to fossil-fuelled internal combustion engines (ICEs), whose fluid-dynamics aspects were deeply investigated in the past years thanks to advanced numerical models. This technology has several interesting properties such as high

* Corresponding author: giuseppe.corda@outlook.it

efficiency, low operating temperatures, quiet operation, quick start-up capability, and simplicity of design. In addition, hydrogen-powered fuel cell electric vehicles (FCEVs) have the potential to provide zero-emission full-electric mobility by eliminating the well-known problem of battery recharging time. Nonetheless, there are still some issues concerning in-vehicle storage systems, such as the high energy demand for compression in the case of gaseous and liquid storage, as well as those related to hydrogen production, which may lead to carbon dioxide production if renewable energies are not used or CO_2 capture is not implemented. Therefore, optimisation of the cost/performance of fuel cells, production and storage systems is necessary before this technology can be adopted on a large scale.

In this respect, the modification of the flow field design towards an interdigitated layout has reported good results in terms of performance increase, as reported in [1]. Indeed, the current density limit is related to mass transport limitations, which depend on the porosity and tortuosity of the porous layers and the amount of liquid water present. If the latter is not effectively removed from the cell, the so-called *flooding* phenomenon occurs, obstructing the effective transport of reactants to the catalyst layer. The interdigitated layout is a promising solution to the issue, thanks to the additional contribution of the forced convective transport mechanism, removing the liquid from the active sites and allowing higher transport rates of the gaseous reactant species to the catalytic layer. This phenomenon increases the limiting current density at low voltages, because of the suppression effect of the concentration overpotential. Mathematical modelling is an important tool for the development and optimisation of fuel cells, and several studies carried out on interdigitated layouts are reported in the literature, such as that reported by Yi and Nguyen [2] that developed a two-dimensional, steady-state, multi-component transport model to simulate the transports of gases in the cathode side of PEMFCs. Um et al [3] conducted a comparative three-dimensional computational study for PEMFC with conventional and interdigitated flow fields. In addition, a three-dimensional steady-state mathematical model was reported by Hu et al [4], where the effect of straight-channel and interdigitated flow fields on species transport and electrochemical reactions is investigated. In this work, a three-dimensional multiphase model is used for the analysis of species concentration and liquid phase distribution in porous media for geometry with straight and interdigitated flow fields. Finally, the influence of these results on the production of electric current is analysed by comparing the polarisation curves for the two different geometries.

Mathematical Model

The Mixture Multi-Phase model (MMP) method is used to consider the presence of multiple phases, where it is assumed that the two fluid phases are miscible and at equilibrium, and their motion can be simulated as that of a unique continuum. In particular, a single continuity, momentum and energy equation is solved for the Eulerian mixture, and the phases subdivision is handled by a dedicated transport equation for the volume fraction and the phase relative velocity [5] and used to numerically investigate multi-phase processes in PEMFC [6-8]. In this study, the governing equations are simplified and solved by using the following assumptions:

1. Laminar flow.
2. Both the fuel and oxidant gases are considered ideal gases.
3. The gravity effect is ignored.

4. The gas diffusion layer and catalyst layer are isotropic and homogeneous, characterized by effective permeability, uniform porosity, and tortuosity.
5. Butler–Volmer kinetics governs the electrochemical reaction.
6. The membrane is impermeable to gaseous species.
7. Steady-state approach.

Governing equations

The transport equations are given below assuming the steady-state case, i.e. where the term $\frac{\partial}{\partial t} = 0$.

Continuity:
$$\nabla(\rho_{mix}\vec{u}_{mix}) = S_m \quad (1)$$

Momentum:
$$\nabla\left(\frac{\rho_{mix}\vec{u}_{mix}\vec{u}_{mix}}{\varepsilon^2}\right) = -\nabla p + \mu\nabla\left[\nabla\left(\frac{\vec{u}_{mix}}{\varepsilon}\right) + \nabla\left(\frac{\vec{u}_{mix}^T}{\varepsilon}\right)\right] - \frac{2}{3}\mu\nabla\left[\nabla\left(\frac{\vec{u}_{mix}}{\varepsilon}\right)\right] + \mathrm{S_u} \quad (2)$$

Species:
$$\nabla(\rho_{mix}Y_i\vec{u}_{mix}) = \nabla\left(\rho D_i^{eff}\nabla \mathrm{Y_i}\right) + \mathrm{S_i} \quad (3)$$

Energy:
$$\nabla\left[\left(\rho_{mix}c_p\right)^{eff}\vec{u}_{mix}T\right] = \nabla(k^{eff}\nabla T) + S_T \quad (4)$$

Charge:
$$\nabla(\kappa^{eff}\nabla\varphi_s) + S_{\varphi_s} = 0 \quad (5)$$
$$\nabla(\sigma^{eff}\nabla\varphi_e) + S_{\varphi_e} = 0 \quad (6)$$

Modeling of membrane

The membrane is modelled as a solid part, thus preventing the transit of gaseous species while allowing the displacement of ions and liquid water (via electro-osmotic effect) in the absorbed phase. For the conductivity of the membrane, the correlation proposed by Springer [9] is used, as a function of the water content of the membrane (λ) and temperature:

$$\sigma_\mathrm{m} = (0.5139\lambda - 0.326)\cdot\exp\left[1268\left(\frac{1}{303} - \frac{1}{\mathrm{T}}\right)\right] \quad (7)$$

Where the water content of the membrane at equilibrium can be expressed by correlation [10]:

$$\lambda_{\mathrm{eq}} = \begin{cases} 0.043 + 17.81\mathrm{a} - 39.85\mathrm{a}^2 + 36.0\mathrm{a}^3 \text{for } 0 < \mathrm{a} < 1 \\ 14 + 1.4(\mathrm{a}-1) \text{for } 1 \le \mathrm{a} \le 3 \end{cases} \quad (8)$$

Modeling approach for Catalyst Layer

A macro-homogeneous model was chosen for modelling CL. This approach considers the CL as a layer of finite thickness, with averaged transport coefficients describing the effect of variations in compositional parameters describing platinum catalyst, carbon support, solid GDL matrix, and electrolyte materials [11]. This type of modelling allows electrochemical reactions to be simulated on the internal surface of the component, making it possible to visualise the distribution of the reaction rate over the entire volume.
The volumetric transfer currents j_a and j_c are given by the Butler–Volmer Equation:

$$\mathrm{j_c} = \zeta \cdot \mathrm{j_{0,c}^{ref}} \cdot \left(\frac{\mathrm{c_{O_2}}}{\mathrm{c_{O_2}^{ref}}}\right)^{\gamma_c} \cdot \left[-\mathrm{e}^{\left(\frac{\alpha_a F \eta_c}{RT}\right)} + \mathrm{e}^{\left(-\frac{\alpha_c F \eta_c}{RT}\right)}\right] \tag{9}$$

$$\mathrm{j_a} = \zeta \cdot \mathrm{j_{0,a}^{ref}} \cdot \left(\frac{\mathrm{c_{H_2}}}{\mathrm{c_{H_2}^{ref}}}\right)^{\gamma_a} \cdot \left[\mathrm{e}^{\left(\frac{\alpha_a F \eta_a}{RT}\right)} - \mathrm{e}^{\left(-\frac{\alpha_c F \eta_a}{RT}\right)}\right] \tag{10}$$

Where the specific active surface of the catalyst $\zeta[m^{-1}]$ is modelled by:

$$\zeta = \frac{\mathrm{A_s m_{pt}}}{\delta_{\mathrm{CL}}} \tag{11}$$

Two different solid phases were used to model the component, namely an ionomer phase (equivalent to that used in the membrane and responsible for the ion transport) and a Pt/C phase (on which the electrochemical reactions and electron transport take place).

Table 1 Source terms for the mixture multi-phase (MMP) governing equations from [11].

	GC	**GDL**	**CL**	**Solid Parts (Mem & BP)**
Mass	$S_m = 0$	$S_m = 0$	$S_m = \sum_i S_i$	$\vec{u}_{mix} = 0$
Momentum	$S_u = 0$	$S_u = \left(-\frac{\mu}{K_{GDL}}\right)\vec{u}_{mix}$	$S_u = \left(-\frac{\mu}{K_{CL}}\right)\vec{u}_{mix}$	$\vec{u}_{mix} = 0$
Species	$S_i = 0$	$S_i = 0$	$S_{H_2,a} = -\frac{j_a}{2F} M_{H_2}$ $S_{H_2O,a} = -\nabla\left[\frac{n_d}{F}\sigma^{eff}\nabla\varphi_e\right]\mathrm{M_{H_2O}}$ $S_{O_2,c} = -\frac{j_c}{4F} M_{O_2}$ $S_{H_2O,c} = \frac{j_c}{2F} M_{H_2O} + \nabla\left[\frac{n_d}{F}\sigma^{eff}\nabla\varphi_e\right]\mathrm{M_{H_2O}}$	$Y_i = 0$
Energy	$S_T = 0$	$S_T = \frac{i_s^2}{\kappa^{eff}}$	$S_{T,a} = j_a\lvert\eta_{act}\rvert + \frac{i_s^2}{\kappa^{eff}} + \frac{i_e^2}{\sigma^{eff}}$ $S_{T,c} = j_c\lvert\eta_{act}\rvert + \frac{j_c T\nabla S}{2F} + \frac{i_s^2}{\kappa^{eff}} + \frac{i_e^2}{\sigma^{eff}}$	$S_T = \frac{i_s^2}{\kappa^{eff}}$ $S_T = \frac{i_e^2}{\sigma^{eff}}$

Charge	$\varphi_s = 0$	$S_{\varphi_s} = 0$	$S_{\varphi_s,a} = -j_a S_{\varphi_e,c} = j_a$	$S_{\varphi_s} = 0$
	$\varphi_e = 0$	$S_{\varphi_e} = 0$	$S_{\varphi_s,c} = j_c \quad S_{\varphi_e,c} = -j_c$	$S_{\varphi_e} = 0$

Computation domain

Numerical simulations are performed on the geometry proposed in the article by Um et al. [3], generating a three-dimensional hexahedral grid using the commercial software STAR-CCM+ from SIEMENS DISW, consisting of approximately 253K finite volume cells. Extrusions at inlets/outlets are added to ensure fully developed flows in the domain of interest. Figure 1 shows the calculation grid for the compared cases and lists the main dimensions.

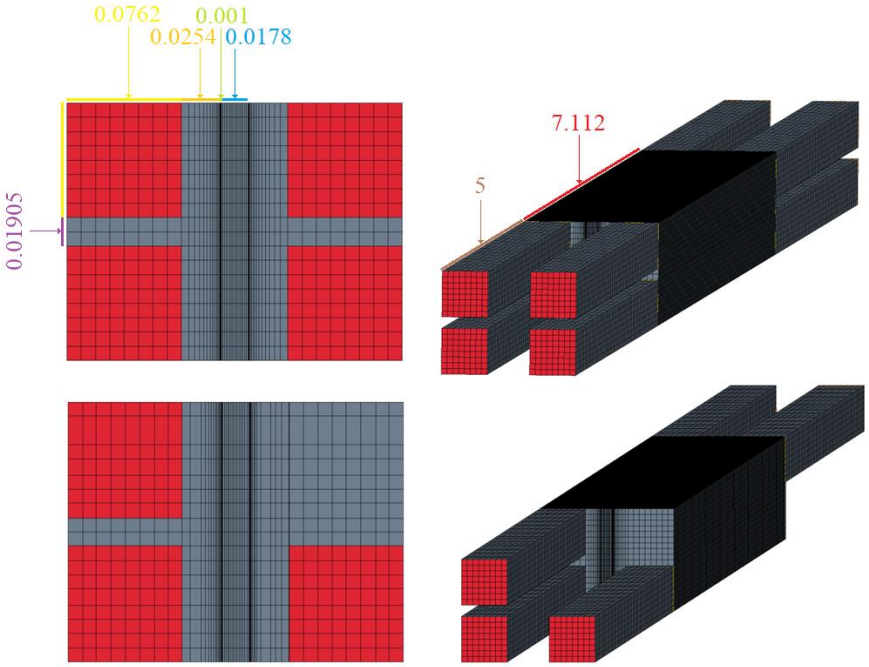

Design Parameters

Description	Value [cm]
Cell Length	7.112
Gas Channel Height	0.0762
Gas Channel Width	0.0762
GDL Thickness	0.0254
CL Thickness	0.001
MEM Thickness	0.0178
Current Collector Width	0.01905
Extrusion	5

Fig.1. Calculation grid and dimensions.

Table 3 Physical properties of Fuel Cell's main components.

Region	**Gaseous species**	**Property**	**Value**
Anode Channel	H_2 H_2O	Relative Humidity	100%
		Molecular Diffusivity $[m^2/s]$	H_2: $1.1 \cdot 10^{-4} H_2O$: $7.35 \cdot 10^{-5}$
		Absolute Pressure $[Pa]$	250.000
Cathode Channel	O_2 N_2 H_2O	Relative Humidity	100%
		Molecular Diffusivity $\left[\frac{m^2}{s}\right]$	O_2: $3.3 \cdot 10^{-5} N_2$: $4 \cdot 10^{-5}$
		Absolute Pressure $[Pa]$	250.000
GDL		Electrical Conductivity $[S/m]$	1000
		Porosity ε	0.4
		Tortuosity τ	$1 + 0.72 \frac{1-\varepsilon}{(\varepsilon-0.11)^{0.54}}$
CL		Volume Fraction of Ionomer	0.2
		Volume Fraction of Pt/C	0.8
		Electrical Conductivity $[S/m]$	1000
		Porosity ε	0.2
		Tortuosity τ	$1 + 0.72 \frac{1-\varepsilon}{(\varepsilon-0.11)^{0.54}}$

Table 4 Boundary conditions

Domain	**Surface**	**Property**	**Value**
Anode Channel	Inlet	Species Mole Fraction	H_2: 0.83
			H_2O : 0.17
		Velocity $[m/s]$	3
		Temperature $[K]$	353
	Outlet	Species mole fraction	H_2: 0.83
			H_2O : 0.17
		Absolute Pressure $[Pa]$	250.000
		Temperature $[K]$	353
Cathode Channel	Inlet	Species Mole Fraction	O_2: 0.1
			H_2O : 0.17
			N_2: 0.73
		Velocity $[m/s]$	3
		Temperature $[K]$	353

	Outlet	Species Mole Fraction	O_2: 0.1
			H_2O : 0.17
			N_2: 0.73
		Absolute Pressure $[Pa]$	250.000
		Temperature $[K]$	353
Bipolar Plates	External Surface BP Anode	Electric Potential $[V]$	0
	External Surface BP Cathode	Electric Potential $[V]$	From OCV to 0.3

Table 5 Material properties of Fuel Cell's electrodes.

Physics	**Property**	**Value**
Anode:	Exchange Current Density $[A/m^2]$	$230 \cdot \left(\frac{C_{H_2}}{C_{H_2}^{ref}}\right)^{0.5}$
$H_2 \rightarrow 2H^+ + 2e^-$	Specific active surface $[1/m]$	$5.5 \cdot 10^5$
	Charge Transfer Coefficient	$\alpha_a = 1 \mid \alpha_c = 1$
Cathode:	Exchange Current Density $[A/m^2]$	$3.5 \cdot 10^{-4} \cdot \left(\frac{C_{O_2}}{C_{O_2}^{ref}}\right) \cdot exp\left(-8419 \cdot \left(\frac{1}{T} - \frac{1}{353}\right)\right)$
$\frac{1}{2}O_2 + 2H^+ + 2e^- \rightarrow H_2$	Specific active surface $[1/m]$	$5.5 \cdot 10^5$
	Charge Transfer Coefficients	$\alpha_a = 1 \mid \alpha_c = 1$

Results

This section will describe the results obtained in terms of current density, transport of the reactant species in the porous media and management of the liquid phase within the cell for both geometries analysed.

Oxygen concentration in cathode-side porous media

The analysis of the molar concentration of oxygen in the porous media on the cathode side shows that the interdigitated flow field produces higher concentrations than the straight flow-fields in the under-rib area. This phenomenon is more pronounced at low voltages, where the reaction rate is higher. The convective transport mechanism due to the interdigitated geometry allows more efficient transport of the reactant species in the diffusive and catalyst layers, a phenomenon that becomes more evident when the consumption of the reactants is higher, and a diffusive-only transport would not guarantee the same level of reactant supply. In Figure 2(a) and (b) it can be seen that the interdigitated geometry forces gases through the porous media, thus enriching the critical land zone with reactant species. This allows more effective use of the active sites, leading to the

achievement of higher current density as will be demonstrated by the comparison of the polarization curves.

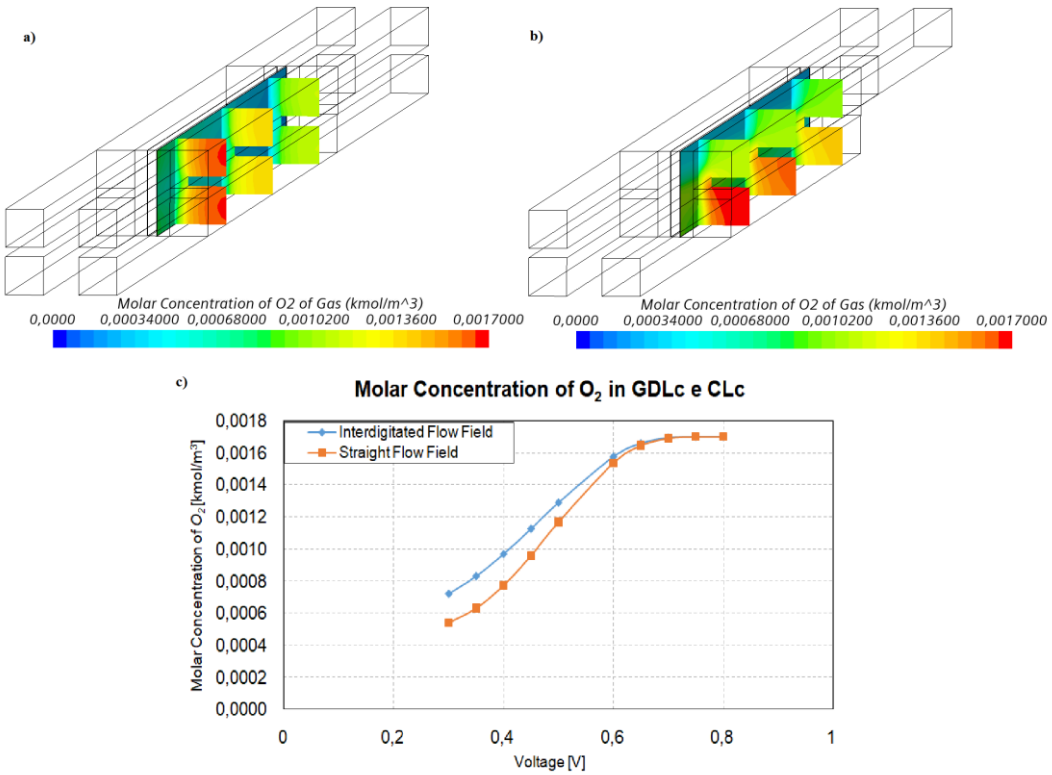

***Fig. 2a*).** Molar concentration of oxygen for straight flow field, **b).** Molar concentration of oxygen for interdigitated flow field, **c).** Volumetric average of the molar concentration of oxygen in GDLc and CLc

Figure 2 c) shows the volumetric average of the oxygen concentration in GDLc and CLc at all simulated voltages, where it is possible to appreciate a variety of curvature at low voltages: this indicates that the limiting condition for species transport is delayed for the interdigitated design.

Liquid phase management

Concerning the management of the liquid phase, shown in Figure 3 a)and *b)*, it is possible to note a uniform presence of liquid in the case of straight channels, while for the interdigitated case the crossing of the gas in the diffusive layers leads to better disposal of the liquid phase, freeing the pores and thus allowing a better transport of the gaseous reactant species, confirming the outcomes of the previous section regarding the molar concentration of oxygen. It should be pointed out that the scale in Figure 3 b) has been reduced by a factor of five to ensure good visualisation of the scalar field. From the latter it is immediate to appreciate how the interdigitated flow effectively removes the liquid

present in the diffusive layer, thus freeing the active sites and strongly reducing the onset of *flooding* phenomenon.

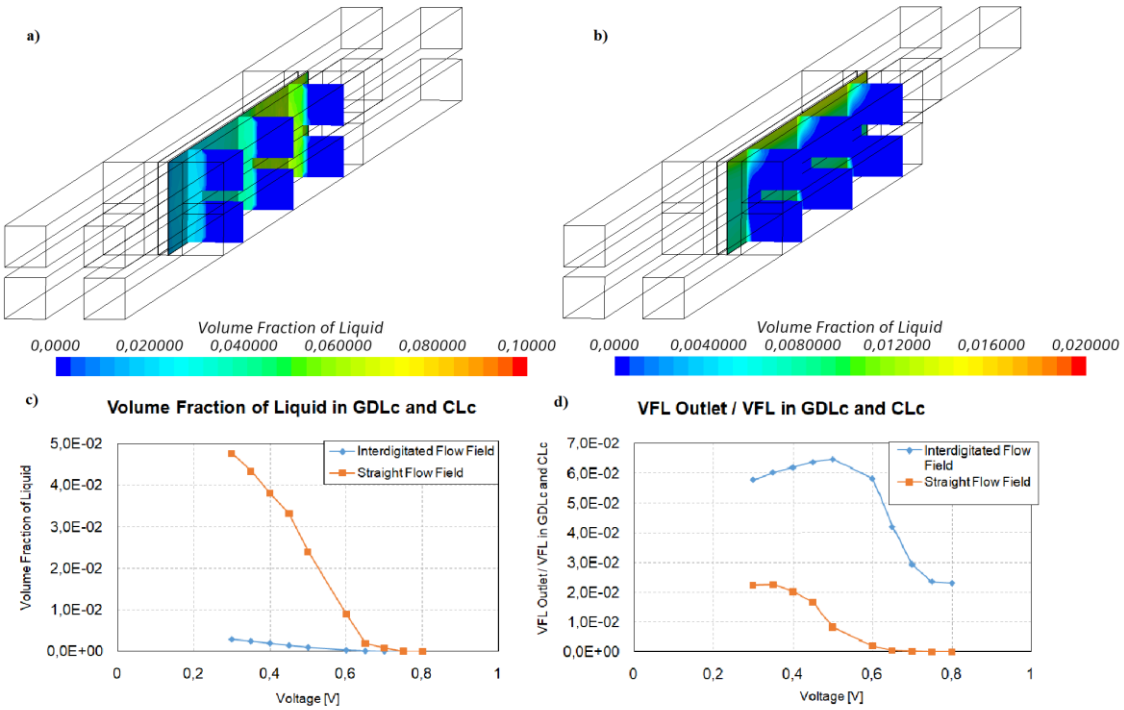

Fig. 3 a) Volume fraction of liquid for straight flow field, **b)** Volume fraction of liquid for interdigitated flow field, **c)**Volumetric average of the volume fraction of liquid in GDLc and CLc, **d)** Ratio between the volume fraction of liquid at the outlet surface and volumetric average of the volume fraction of liquid in GDLc and CLc.

Figure 3 c) shows the graphs of the volumetric average of the liquid volume fraction in the GDLc and CLc. The presence of liquid is greater in both zones for the straight channel case and observing the ratio of the volume fraction of liquid between the outlet and the porous media, shown in Figure 3 d), the greater disposal operated by the interdigitated geometry is confirmed for all the simulated voltages. It is worth noting that the reduction between the difference of the two curves at voltages lower than 0.5 is probably due to the higher liquid production for the interdigitated case (i.e., higher reaction rates); nevertheless, a higher ratio is guaranteed for the interdigitated case than for the straight channel case, confirming a reduced persistence of liquid in the simulated domain and a more efficient removal rate.

Polarization curve

Analysing the polarisation curve shown in Figure 4 a), an increase in performance can be seen in the case of interdigitated channels. At voltages below 0.5V, a difference in the current density delivered by the cell is well noticeable. Whereas at higher voltages the

dominant losses are due to the activation overpotential and ohmic losses, at lower voltages the cell performance is mostly limited by mass transport processes, here optimized in the interdigitated design. In this PEMFC working regime, the interdigitated geometry shows a positive effect on performance due to the more efficient transport of the reactant species in the catalyst zone. Figure 4 b) shows the polarisation curves obtained by Um et al [3] for a conventional and interdigitated geometry. Despite the different values of the current, due to a different modelling approach, a similar trend of the polarization curves can be noticed.

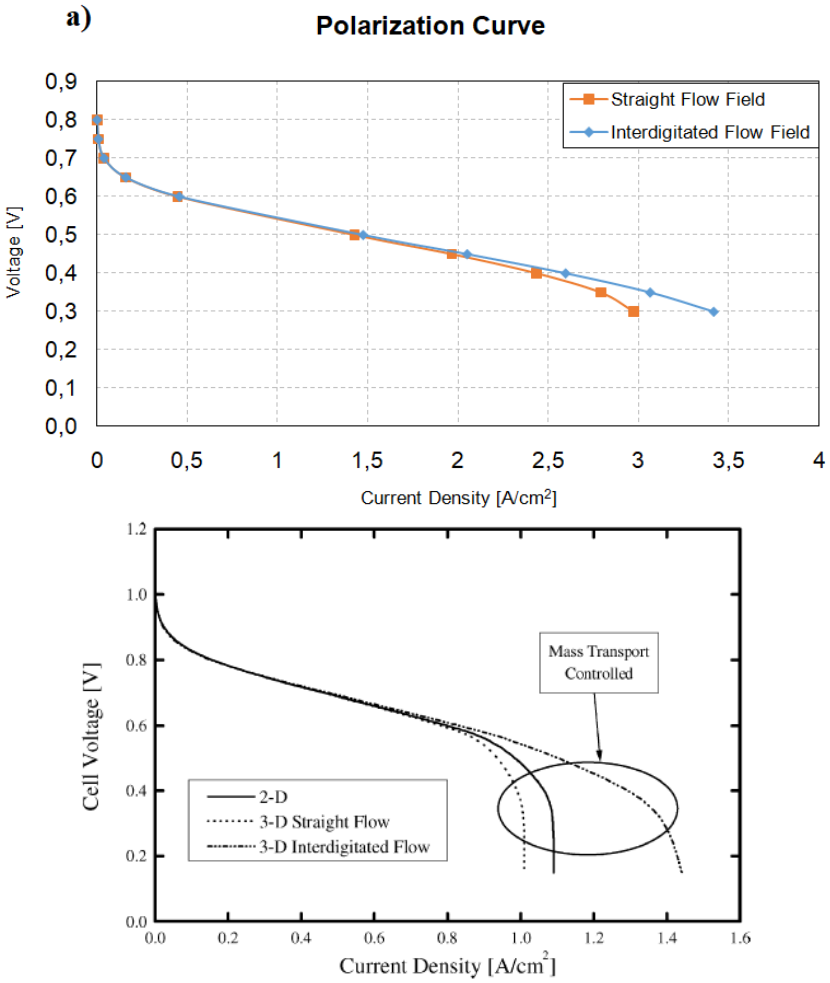

Fig. 4 a) Polarization curves for the straight and interdigitated cases, **b)** Polarisation curves provided by Um and Wang [3]

Conclusions

In this study, a comparison between a straight and an interdigitated flow field is performed using a CFD-3D approach, which allows a comprehensive analysis of oxygen transport and water removal in the three-dimensional domain of a PEMFC. In particular, the

interdigitated flow field shows better performance in the transport of reactant species in the diffusive layers due to a greater effect of convective transport. This promoted reactant supply leads to higher reaction rates, leveraging a more effective transport to the active sites, allowing to achieve higher current densities. In addition, the forced gas flow in the porous layers ensures greater liquid disposal, thus reducing the likelihood of flooding. The analysis of the polarization curve quantitatively confirms the reduction of the concentration overpotential on the interdigitated case, which can provide higher current densities at low voltages.

References

1. A. Kazim et al.,J. Appl. Electrochem. 29 (**1999**), https://doi.org/10.1023/A:1003867012551
2. J.S. Yi et al., J Electrochem Soc **1999**;146:38–45, https://doi.org/10.1149/1.1391561
3. S. Um, C.Y. Wang, Journal of Power Sources 125 (**2004**) 40–51, https://doi.org/10.1016/j.jpowsour.2003.07.007
4. Hu, G. et al. *Journal of Power Sources*, *136*(1), **2004**, https://doi.org/10.1016/j.jpowsour.2004.05.010
5. d'Adamo, A., et al. Processes 2021, 9(4), 688; https://doi.org/10.3390/pr9040688
6. Riccardi, M., et al. E3S Web Conf. Volume 197, **2020**, https://doi.org/10.1051/e3sconf/202019705004
7. D'Adamo, A. et al., SAE Technical Paper 2020-24-0016, **2020**, https://doi.org/10.4271/2020-24-0016.
8. A. d'Adamo et al., Processes **2021**, 9(3), 564; https://doi.org/10.3390/pr9030564
9. T.E. Springer et al., J. Electrochem. Soc. 136 (**1991**) 334.
10. T.E. Springer et al., J. Electrochem. Soc. 138 (**1991**) 2334.
11. Khajeh-Hosseini-Dalasm, N. et al., Int. J. Hydrog. Energy **2010**, 35, https://doi.org/10.1016/j.ijhydene.2009.12.111

Nomenclature

BP: Bipolar Plate
CL: Catalyst Layer
CFD: Computational Fluid Dynamics
FCEV: Fuel Cell Electric Vehicle
GC: Gas Channel
GDL: Gas Diffusion Layer
ICE: Internal Combustion Engine
PEM: Proton Exchange Membrane
PEMFC: Proton Exchange Membrane Fuel Cell

Greek Symbols

α: charge transfer coefficient
γ: pressure scaling coefficients
δ: thickness
ε: porosity
ζ: specific active surface of the catalyst
η: overpotential
κ: electric conductivity
λ: water content
μ: dynamic viscosity
ρ: density
σ: ionic conductivity
τ: tortuosity
φ: potential